ISCI, Volume *16*

Supplemental Information

Completely Solvent-free Protocols to Access Phase-Pure, Metastable Metal Halide Perovskites and Functional Photodetectors from the Precursor Salts

Zonghan Hong, Davin Tan, Rohit Abraham John, Yong Kang Eugene Tay, Yan King Terence Ho, Xin Zhao, Tze Chien Sum, Nripan Mathews, Felipe García, and Han Sen Soo

Supplemental Information

Supplemental data

Table S1. Detailed evaluation of the state-of-the-art in mechanochemical synthesis of metal halide perovskites. Related to Table 1.

Citation in manuscript	Perovskites prepared	Stability or post-synthetic processing methods	Focus of study	Application
(Karmakar et al., 2018)	$MAPbBr_xCl_{3-x}$	All thermally stable phases	Solid-state ^{207}Pb NMR spectroscopy correlated to crystal structures	None
(Pal et al., 2018)	3D $CsPbBr_3$, 2D $CsPb2Br_5$, 0D Cs_4PbBr_6, 3D $CsPbCl_3$, 2D $CsPb_2Cl_5$, 0D Cs_4PbCl_6, 3D $CsPbI_3$, and 3D $RbPbI_3$	All thermally stable phases	Pb-based perovskites of all dimensions from 3D to 0D prepared; interconversion between dimensions by mechanochemistry	None
(Jana et al., 2017)	$APbBr_3$ (A = Cs, MA, FA)	All thermally stable phases, octylammonium surfactants used to stabilize nanoparticles	Different bulk microcrystalline morphologies; access to nanoparticles	None
(Askar et al., 2018)	$FAPbX_3$ (X = Cl, Br, I) and their mixed halides	Mostly thermally stable phases; some metastable examples accessed by post-synthetic annealing	Solid-state ^{207}Pb NMR spectroscopy correlated to crystal structures	None
(El Ajjouri et al., 2018a)	$Cs_{1-x}K_xPbBr_{3-y}X_y$ (X = I, Br, Cl)	All thermally stable phases	Use of K cations to passivate traps	None
38(El Ajjouri et al., 2018b)	$CsPbX_3$ (X = Cl, Br, I)	All thermally stable except $CsPbI_3$; vaporization and thermal annealing to access thin films	Use of single sources for vacuum deposition of mechanochemically prepared perovskites	None
(Prochowicz et al., 2018)	$CsPbCl_3$, $CsPbBr_3$, $CsPbBr_{1.5}Cl_{1.5}$, and mixed ion $FA_xMA_{1-x}CsPbI_yBr_{3-y}$	All thermally stable phases; post-synthetic solution processing in DMSO/DMF to prepare solar cells	High efficiency solar cells with Cs additives derived from mechanochemically prepared powders	Solar cell
(Prochowicz et al., 2017)	$MA_xFA_{1-x}PbI_3$	Mostly stable phases; MA added to stabilize α-$FAPbI_3$; solution processing to prepare solar cells	Development of solar cells with perovskites derived from mechanochemistry	Solar cell
(Protesescu et al., 2018)	$FAPbBr_3$ and $CsPbBr_3$	All thermally stable phases, octylammonium surfactants used to stabilize nanoparticles	Mechanochemical synthesis of highly luminescent nanocrystals	None
(Sadhukhan et al., 2018)	$MAPbI_xBr_{3-x}$	All thermally stable phases	Band gap tuning by changing relative halide composition	None
(Yun et al., 2018)	$MAPbBr_3$ and $FAPbBr_3$	All thermally stable phases, octylammonium and octadecylammonium surfactants used to stabilize nanoparticles	Surfactant assisted exfoliation to access luminescent nanocrystals	None
(Posudievsky et al., 2017)	$CsPbBr_3$	Stable nanoparticles, processed in DMF	Nanoparticles prepared by mechanochemistry	None

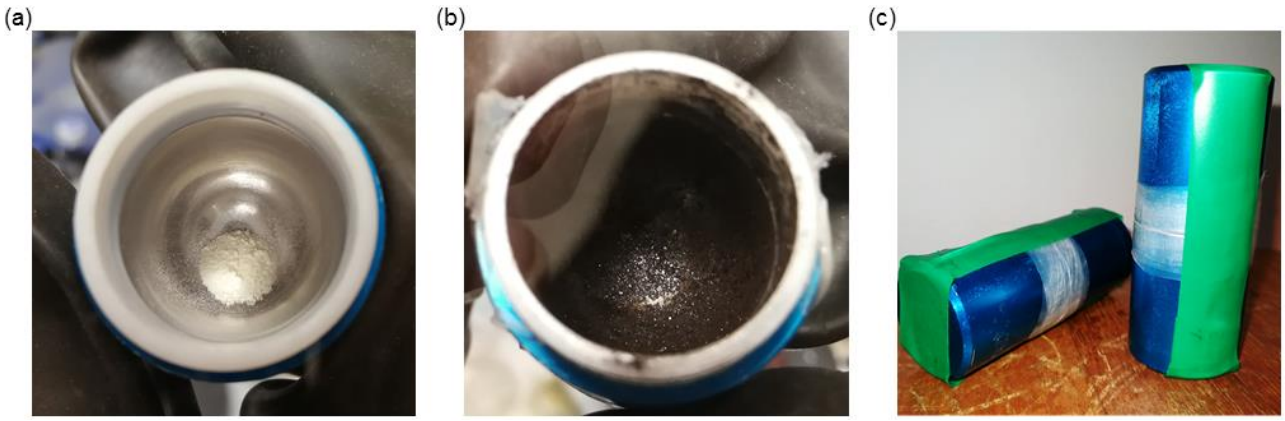

Figure S1. Photographs of the mechanochemical synthesis of $CsSnBr_3$ as an example (a) before and (b) after ball milling; (c) milling jars were sealed with paraffin film and electrical tape to prevent exposure to air. Related to Figure 1.

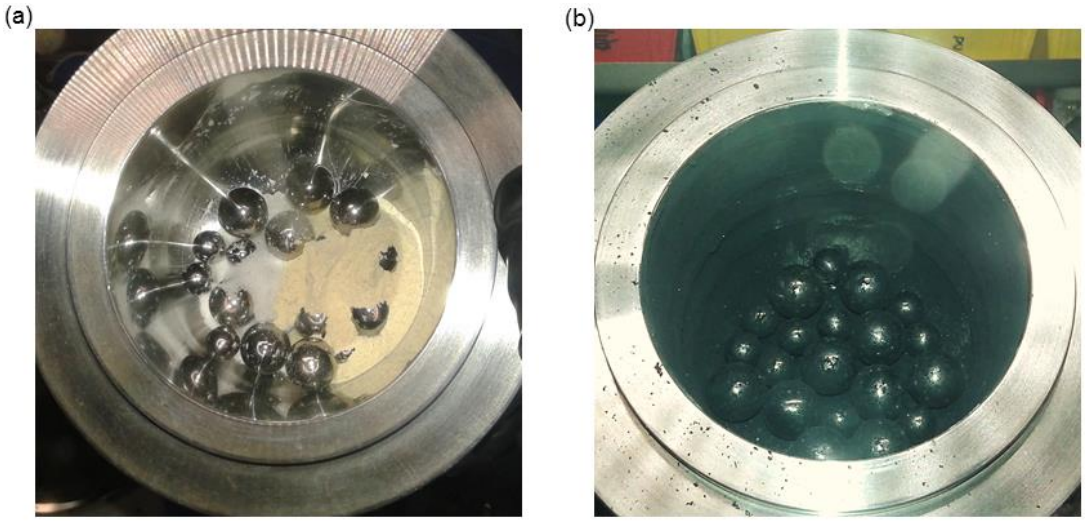

Figure S2. Photographs of the large-scale (25 g) synthesis of $CsSnBr_3$ (a) before and (b) after ball milling. Related to Figures 1 and 4.

Figure S3. Photographic demonstration of the kg-scale synthesis of $CsSnBr_{1.5}Cl_{1.5}$. a) Preparation of the reagents CsBr, CsCl, $SnBr_2$, and $SnCl_2$ (all white powders) in a N_2 glovebox. The reagents were weighed and transferred from a beaker into the 250 mL mechanochemical reaction vessel. The total reagent weight was 250 g. b) The reagent mixture with the milling balls at the bottom of the vessel. c) Gentle mixing of the reagents, which exposed the milling balls, by using a metal spatula. d) Planetary mill containing four reaction vessel holders, essentially allowing four 250 g reactions to take place simultaneously, leading to a 1.0 kg scale batch synthesis of the perovskite. e) The orange product after 10 hr of milling. Related to Figures 1 and 4.

PXRD studies of control experiments

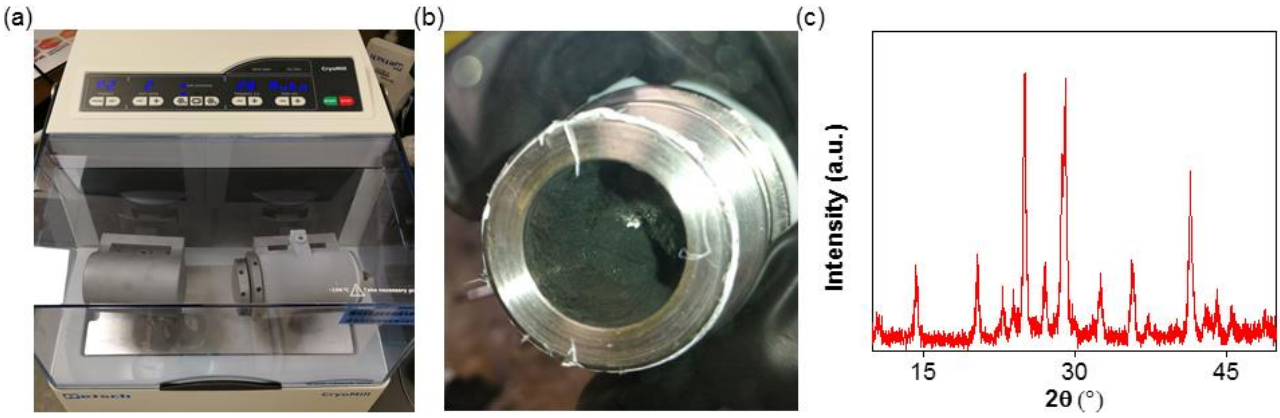

Figure S4. Photographs and data of the cryomilling synthesis of $CsSnI_3$. (a) Photograph of cryomilling setup with liquid N_2 flow. (b) Photograph showing the black perovskite phase product obtained by cryomilling. (c) PXRD pattern of the product from cryomilling, showing a pure orthorhombic (black) phase. Related to Figure 2.

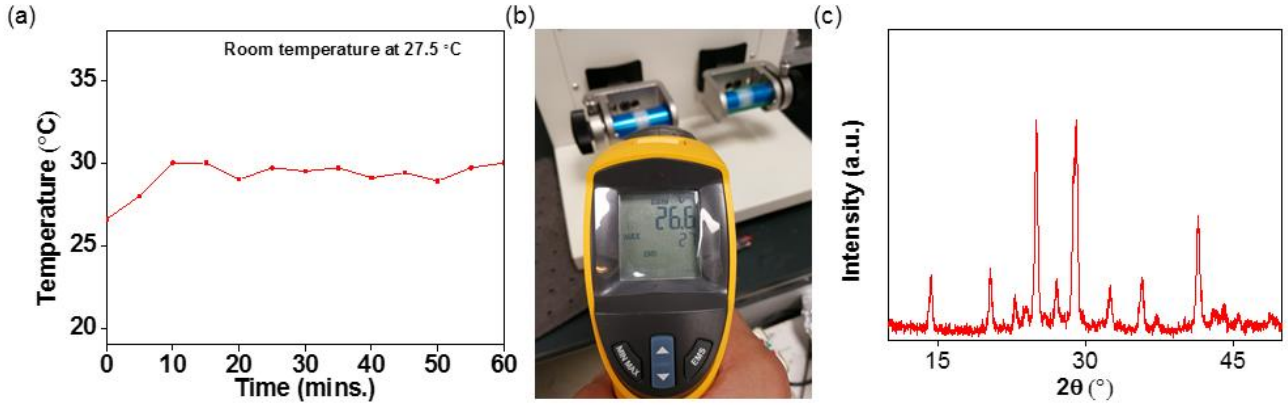

Figure S5. Controlled-temperature mechanochemical synthesis of $CsSnI_3$. (a) Reaction temperature monitored over 1 hr during a milling experiment. The milling jars were then allowed to cool down to below 28 °C every 5 min before the milling resumed. (b) Photograph of a reaction monitored by an IR thermometer. (c) PXRD pattern of the product showing a pure orthorhombic (black) phase. Related to Figure 2.

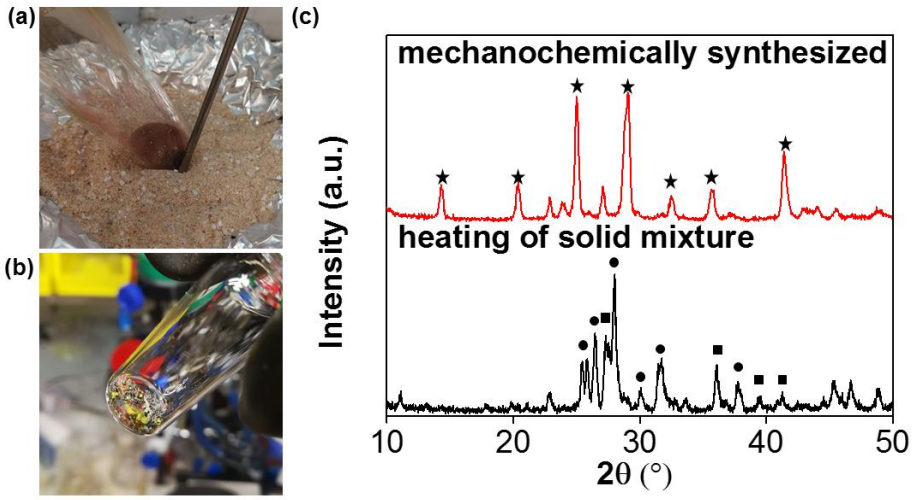

Figure S6. Control experiments for the attempted synthesis of $CsSnI_3$ perovskite with heat only under solvent-free conditions. (a) Photograph of the solid reaction mixture being heated in a sand-bath equipped with a temperature sensor. (b) Photograph of the resulting product after heating to 320 ºC for 1 h, showing a multi–colored solid. (c) Comparison of the PXRD patterns of the perovskite powder that was synthesized mechanochemically (red line) and the heated solid product (black line). Multiple compounds can be identified from the thermal reaction, including SnI_2 and $CsSnI_3$ in the yellow orthorhombic phase as the major components. Related to Figure 2.

XPS experiments and data

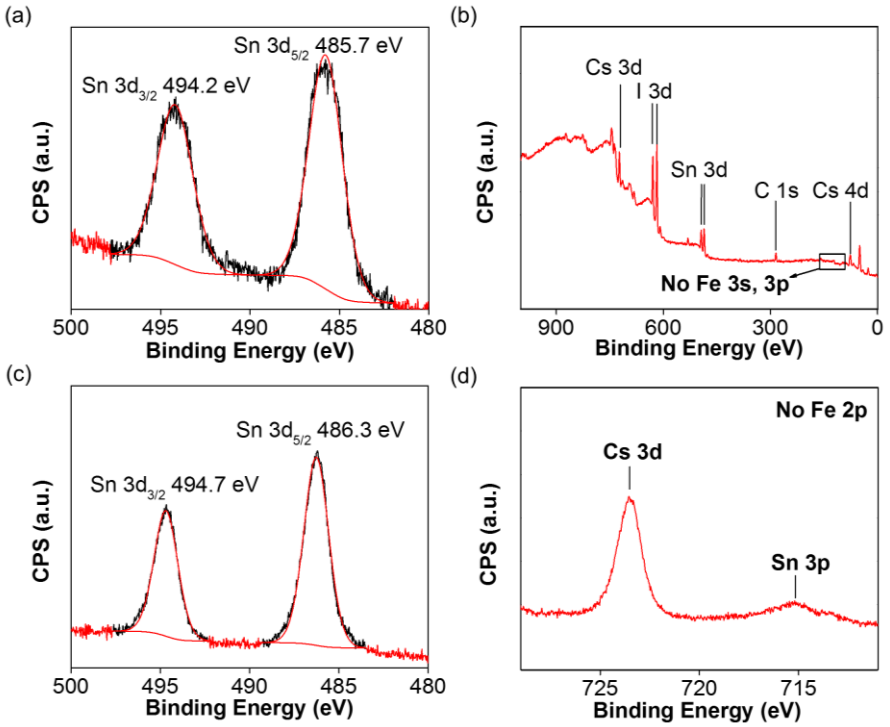

Figure S7. (a) Sn 3d XPS data for $CsSnI_3$. (b) Survey spectrum of $CsSnI_3$. (c) Sn 3d XPS data in $CsSnI_3$ after being exposed to air. (d) no Fe was detected in the 2p range. Related to Figures 2 and 3.

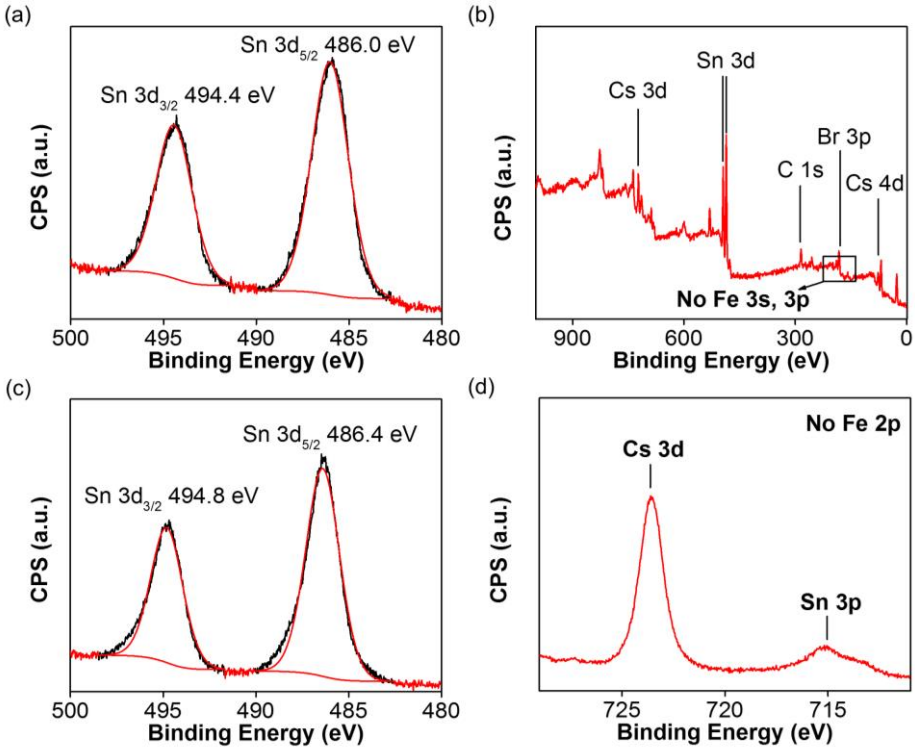

Figure S8. (a) Sn 3d XPS data for $CsSnBr_3$. (b) Survey spectrum of $CsSnBr_3$. (c) Sn 3d XPS data in $CsSnBr_3$ after being exposed to air. (d) no Fe was detected in the 2p range. Related to Figure 4.

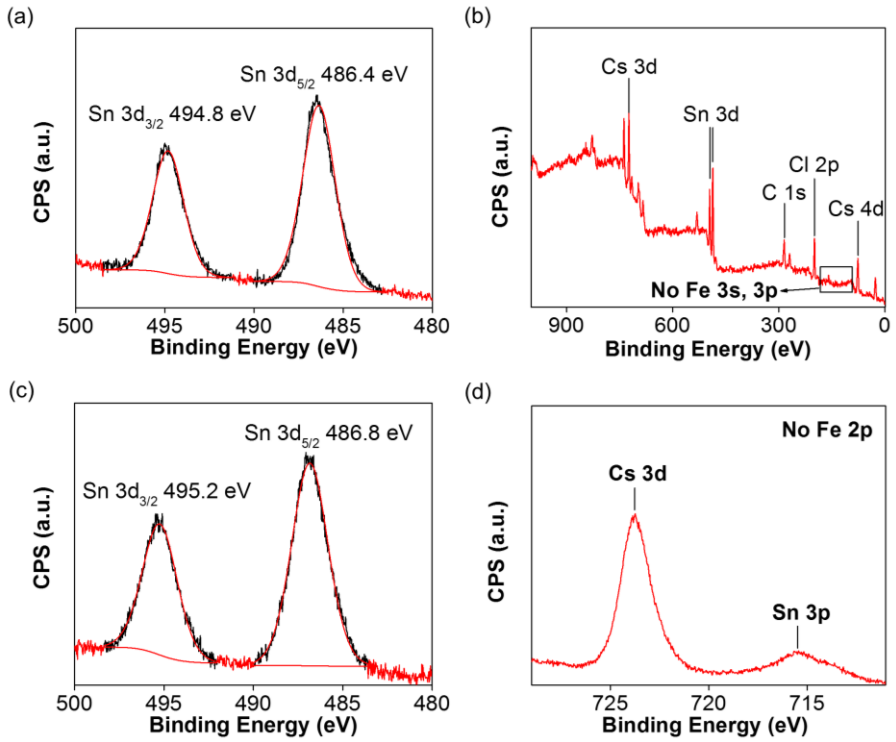

Figure S9. (a) Sn 3d XPS data for $CsSnCl_3$. (b) Survey spectrum of $CsSnCl_3$. (c) Sn 3d XPS data in $CsSnCl_3$ after being exposed to air. (d) no Fe was detected in the 2p range. Related to Figure 4.

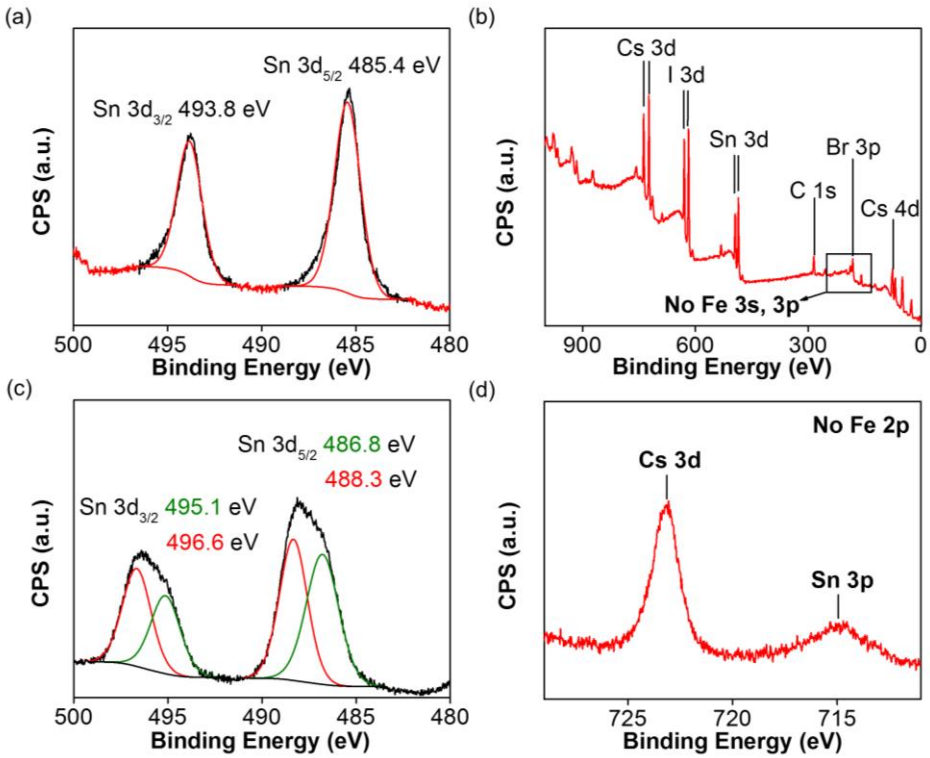

Figure S10. (a) Sn 3d XPS data for $CsSnBr_{1.5}I_{1.5}$. (b) Survey spectrum of $CsSnBr_{1.5}I_{1.5}$. (c) Sn 3d XPS data in $CsSnBr_{1.5}I_{1.5}$ after being exposed to air. (d) no Fe was detected in the 2p range. Related to Figure 4.

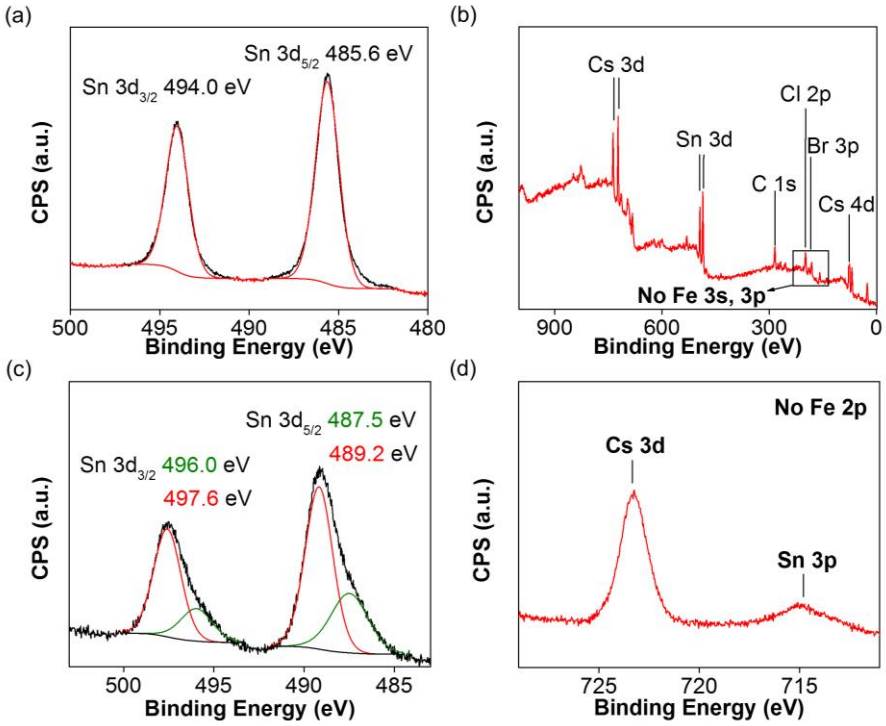

Figure S11. (a) Sn 3d XPS data for $CsSnBr_{1.5}Cl_{1.5}$. (b) Survey spectrum of $CsSnBr_{1.5}Cl_{1.5}$. (c) Sn 3d XPS data in $CsSnBr_{1.5}Cl_{1.5}$ after being exposed to air. (d) no Fe was detected in the 2p range. Related to Figure 4.

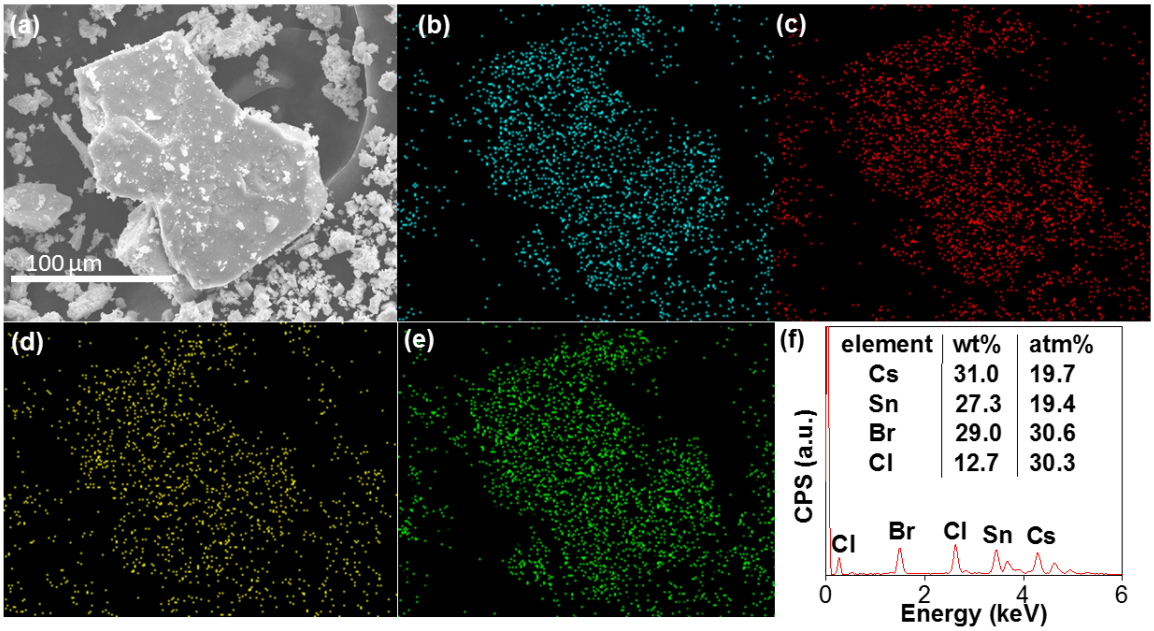

Figure S12. (a) SEM image of the mechanochemically synthesized $CsSnBr_{1.5}Cl_{1.5}$ perovskite, with the EDX analysis of the different elements (b) Cs (blue), (c) Sn (red), (d) Br (yellow), and (e) Cl (green), illustrating that all the elements are homogenously distributed throughout the solid particles. (f) The elemental composition as determined by EDX shows an approximately 1:1:1.5:1.5 molar ratio of Cs:Sn:Br:Cl atoms, which coincides with the chemical formula of $CsSnBr_{1.5}Cl_{1.5}$. It is worth noting that such precise stoichiometry is hard to achieve by solution-based methods. Related to Figure 4.

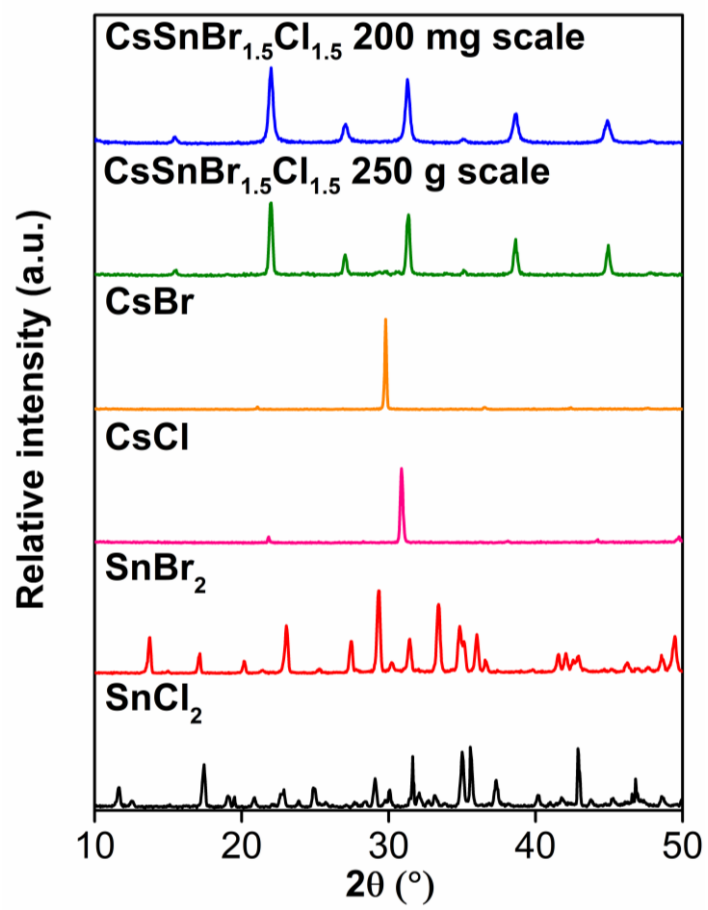

Figure S13. Comparison of the PXRD patterns of $CsSnBr_{1.5}Cl_{1.5}$ perovskite synthesized in 200 mg and 250 g scales, and the CsBr, CsCl, $SnBr_2$, and $SnCl_2$ precursors. The PXRD pattern of the 250 g scale synthesized product is almost indistinguishable from the small scale one and does not contain any precursor peaks. Related to Figures 1 and 4.

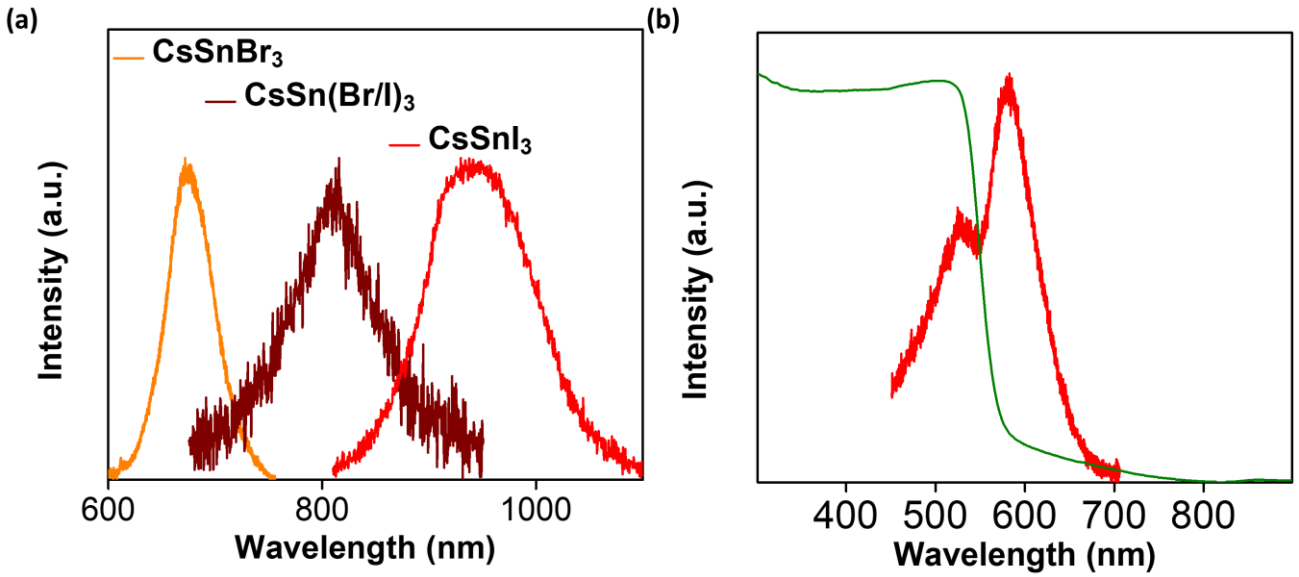

Figure S14. (a) PL data of spin-coated films of $CsSnBr_3$ (orange), $CsSnBr_{1.5}I_{1.5}$ (brown), and $CsSnI_3$ (red). (b) UV-vis DRS (green) and PL (red) data of mechanochemically synthesized $CsSnBr_{1.5}Cl_{1.5}$ powder. Related to Figures 4 and 6.

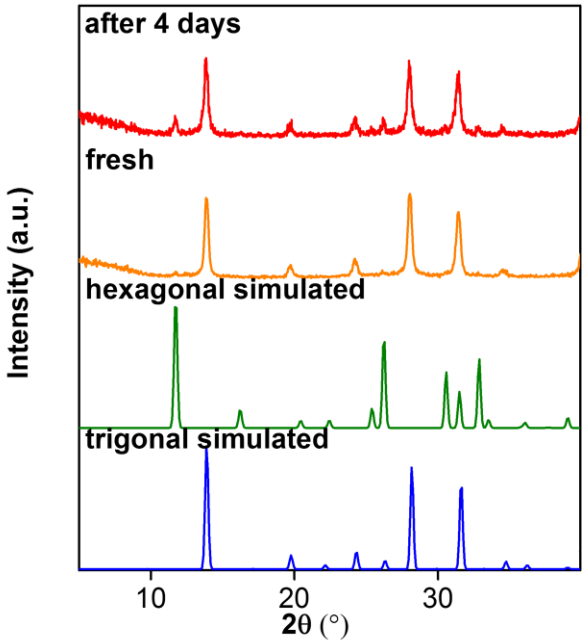

Figure S15. The PXRD patterns of $FAPbI_3$ showing phase transition within 4 days. Related to Figure 5.

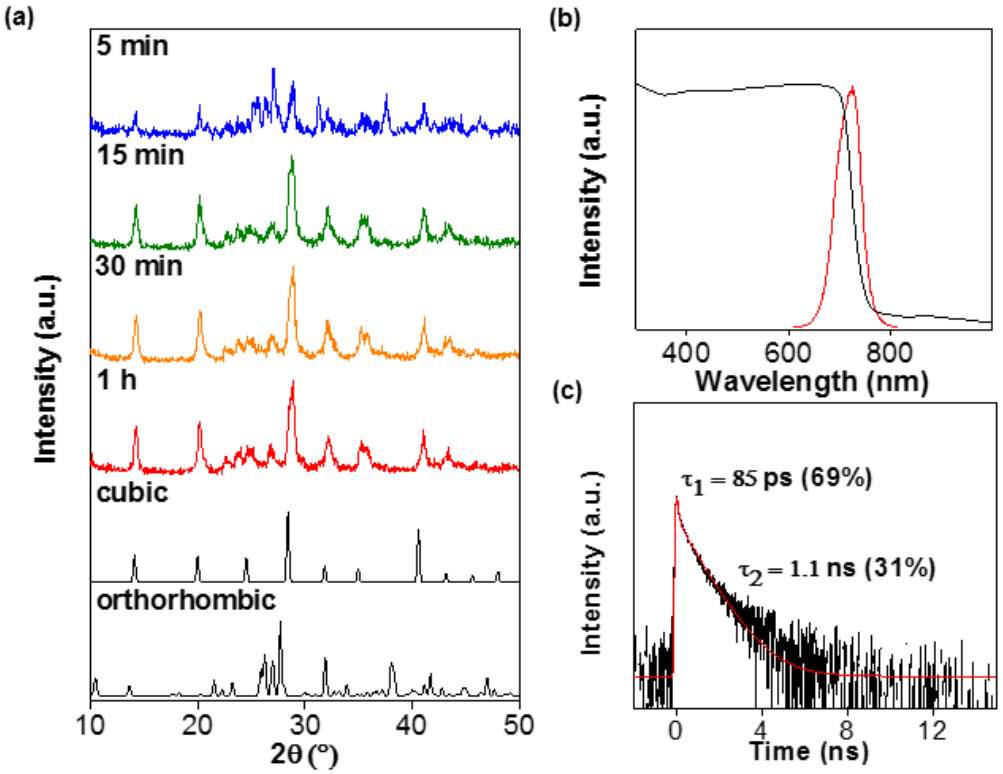

Figure S16. (a) The PXRD patterns of $CsPbI_3$ synthesized with different reaction durations and the simulated patterns for cubic and orthorhombic phases. (b) The UV-vis DRS spectrum (black) and the steady-state PL (red) of $CsPbI_3$. (c) The TRPL spectrum (black) of $CsPbI_3$. The plot was fitted biexponentially (red) to give a short-lived process with a lifetime of 85 ps (69%) and a longer process with a lifetime of 1.1 ns (31%). Related to Figures 5 and 6.

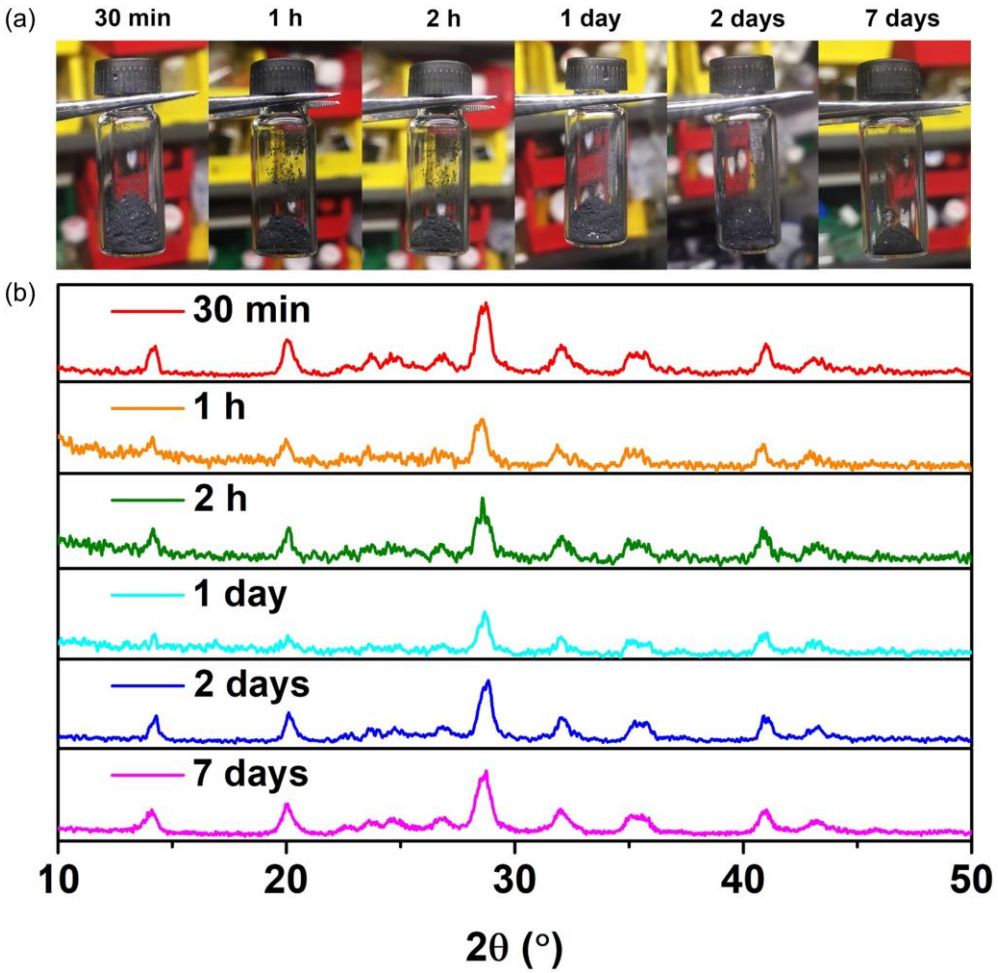

Figure S17. (a) Photographs of the black cubic $CsPbI_3$ synthesized by mechanochemical ball-milling and stored in a glovebox under < 0.5 ppm O_2 and water over seven days. (b) The PXRD pattern of the same mechanochemically prepared black cubic $CsPbI_3$ showing indefinite stability over the course of at least seven days, when stored in an inert atmosphere glovebox. Related to Figures 5 and 6.

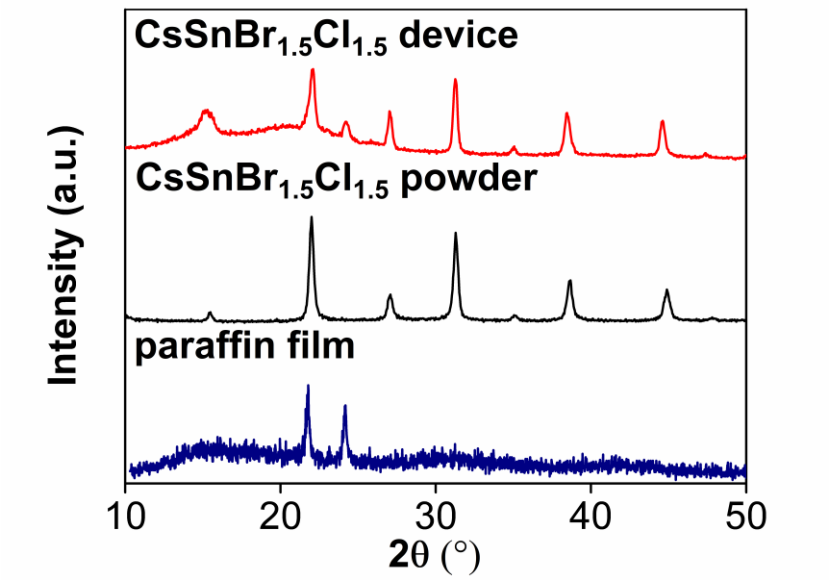

Figure S18. Comparison of the PXRD patterns of the $CsSnBr_{1.5}Cl_{1.5}$ perovskite device after gold electrode deposition with the as-synthesized powder. The peak position at 24° corresponds to the paraffin film that was used to seal the device in order to prevent the exposure to air. Based on the PXRD analysis, there is no significant structural change in the $CsSnBr_{1.5}Cl_{1.5}$ perovskite before and after the process of device fabrication. Related to Figure 7.

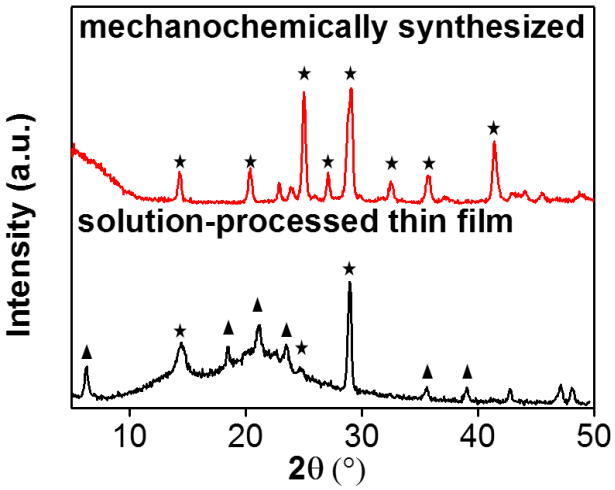

Figure S19. Comparison of the PXRD patterns of the $CsSnI_3$ perovskite that was synthesized mechanochemically (red line), with the sample prepared in solution by heating and spin-coating a thin film onto a glass substrate (black line). The product obtained by solution processing is not pure, since characteristic peaks belonging to the black orthorhombic phase and several other unidentifiable peaks were observed. Related to Figures 2 and 3.

Transparent Methods

Materials.

Cesium chloride (99%), cesium bromide (99.99%), cesium iodide (99.99%), lead iodide (99.999%) and formamidinium iodide (FAI, >99% anhydrous) were purchased from Sigma-Aldrich. Tin(II) chloride (99%) was purchased from Alfa Aesar. Tin(II) bromide (99.9%) was purchased from Sigma-Aldrich and tin(II) iodide (99.99%) was purchased from Strem Chemicals Corp. All the above chemicals were used directly without further purification and stored in a glovebox to minimize the exposure to oxygen. Notably, at the purity levels of the chemicals that we purchased, we did not observe any detectable impurities in the precursor salts that we used based on PXRD measurements (Figures 2e,f and S13). Consequently, no special procedures were necessary in handling the precursors as long as the newly purchased chemicals and the products were opened and handled exclusively in a well-maintained glovebox (O_2 levels < 1 ppm, water levels < 0.5 ppm). This has been further verified since we did not encounter unusual problems beyond the inherent air-, moisture-, and phase-instability of the perovskite products that we studied. Anhydrous dimethyl sulfoxide (DMSO, >99.9%) was purchased from Sigma-Aldrich and stored in a glovebox.

General mechanochemical synthesis procedure.

General procedure for mechanochemical synthesis: Stoichiometric equivalents of precursors (1:1 ratio between cation A^+ and B^{2+}) were mixed in a 25 mL stainless-steel milling jar (Form-Tech Scientific smart snap milling jar) equipped with a stainless-steel milling ball in a glovebox. The milling jar was installed into a shaker mill (Retsch MM400) and the milling was operated at a frequency of 30 Hz for 1 h. The milling jar was then taken into a glovebox, unsealed, and the resulting product was collected. Large scale syntheses were carried out using 250 mL stainless-steel milling jars on a Grinder BM4 planetary mill instead.

$CsSnI_3$: The general procedure was used with the following quantities: cesium iodide (77.9 mg, 0.30 mmol) and tin(II) iodide (112 mg, 0.30 mmol). The resulting product (150 mg, 79% yield) was collected as a black powder.

$CsSnBr_3$: The general procedure was used with the following quantities: cesium bromide (106 mg, 0.50 mmol) and tin(II) bromide (139 mg, 0.50 mmol). The resulting product (225 mg, 92% yield) was collected as a black powder.

$CsSnCl_3$: The general procedure was used with the following quantities: cesium chloride (84.2 mg, 0.50 mmol) and tin(II) chloride (94.8 mg, 0.50 mmol). The resulting product (145 mg, 81% yield) was collected as a yellow powder.

$CsSnBr_{1.5}Cl_{1.5}$: The general procedure was used with the following quantities: cesium bromide (53 mg, 0.25 mmol), tin(II) bromide (70 mg, 0.25 mmol), cesium chloride (42 mg, 0.25 mmol), and tin(II) chloride (47 mg, 0.25 mmol). The resulting product (169 mg, 79% yield) was collected as an orange powder.

$CsSnBr_{1.5}I_{1.5}$: The general procedure was used with the following quantities: cesium iodide (65 mg, 0.25 mmol), tin(II) iodide (93 mg, 0.25 mmol), cesium bromide (53 mg, 0.25 mmol), and tin(II) bromide (70 mg, 0.25 mmol). The resulting product (228 mg, 81% yield) was collected as a black powder.

$CsPbI_3$: The general procedure was used with the following quantities: cesium iodide (130 mg, 0.50 mmol) and lead(II) iodide (230 mg, 0.50 mmol). The mixed powder was ball-milled for 15 min resulting in the product (295 mg, 82% yield) as a black powder.

$FAPbI_3$: The general procedure was used with the following quantities: FAI (57 mg, 0.33 mmol), lead(II) iodide (153 mg, 0.33 mmol), and 0.10 mL of pentane added to assist the ball-milling (liquid assisted grinding, LAG). The mixture was milled for 15 min and the resulting product (168 mg, 80% yield) was collected as a black powder.

Large-scale synthesis:

$CsSnBr_3$ (25 g scale): Cesium bromide (10.6 g, 50 mmol) and tin(II) bromide (13.9 g, 50 mmol) were mixed in a 250 mL stainless-steel milling jar equipped with eight 4.0 g and fifteen 13.5 g stainless-steel milling balls (ball to reactant ratio = 2.35) in a glovebox. The milling jar was then installed into a Grinder BM4 planetary mill with four vessel holders and the milling was operated at 300 revolutions per minute (rpm, sun wheel speed) for cycles consisting of 3 min of continuous milling and a pause for 1 min, followed by a reverse in the rotation direction after each cycle, for a 3 hr total milling duration. The milling jar was then taken into a glovebox, unsealed, and the resulting black product (23.6 g, 94% yield) was collected.

$CsSnBr_{1.5}Cl_{1.5}$ (250 g scale): Cesium bromide (62.6 g, 0.29 mol), cesium chloride (49.6 g, 0.29 mol), tin(II) bromide (81.9 g, 0.29 mol), and tin(II) chloride (55.8 g, 0.29 mol) were mixed in a 250 mL stainless-steel milling jar equipped with fourteen 4.0 g and twenty 13.5 g stainless-steel balls (ball to reactant ratio = 1.30) in a glovebox. The milling jar was then installed into the same planetary mill and operated with the same milling cycles as the 25 g scale above, for a 2+2+2+2+2 = 10 hr total milling duration. Such interval milling was

performed to prevent overheating and reduce wear and tear on the planetary mill. The milling jar was then taken into a glovebox, unsealed, and the resulting black product (241 g, 96% yield) was collected.

Table S2. Synthetic details of the mechanochemically synthesized $CsSnX_3$ (mg scale). Related to Figures 1 and 4.

ABX_3	**Quantity of precursors**	**Product appearance**	**Yield**
$CsSnI_3$	CsI (77.9 mg, 0.30 mmol) SnI_2 (112 mg, 0.30 mmol)	black powder	150 mg, 79%
$CsSnBr_3$	CsBr (106 mg, 0.50 mmol) $SnBr_2$ (139 mg, 0.50 mmol)	black powder	225 mg, 92%
$CsSnCl_3$	CsCl (84.2 mg, 0.50 mmol) $SnCl_2$ (94.8 mg, 0.50 mmol)	yellow powder	145 mg, 81%
$CsSnBr_{1.5}Cl_{1.5}$	CsBr (53 mg, 0.25 mmol) $SnBr_2$ (70 mg, 0.25 mmol) CsCl (42 mg, 0.25 mmol) $SnCl_2$ (47 mg, 0.25 mmol)	orange powder	169 mg, 79%
$CsSnBr_{1.5}I_{1.5}$	CsI (65 mg, 0.25 mmol) SnI_2 (93 mg, 0.25 mmol) CsBr (53 mg, 0.25 mmol) $SnBr_2$ (70 mg, 0.25 mmol)	black powder	228 mg, 81%
$CsPbI_3$	CsI (130 mg, 0.50 mmol) PbI_2 (230 mg, 0.50 mmol)	black powder	295 mg, 82%
$FAPbI_3$	FAI (57 mg, 0.33 mmol) PbI_2 (153 mg, 0.33 mmol) 0.10 mL pentane for LAG	black powder	168 mg, 80%

Fabrication of solution processed samples

General procedure for the fabrication of a thin film sample: 10 µL of a 0.40 M precursor solution in DMSO was spin coated onto a quartz substrate at 4000 rpm for 30 s. In order to obtain high quality films, 100 µL of

toluene were dropped onto the substrate spinning at 4000 rpm for another 30 s. The coated substrate was then placed on a hot plate at 90 °C for 10 min.

Control experiments with heating only under solvent-free conditions

Stoichiometric equivalents of the precursors were mixed and sealed in a 25 mL reaction tube, heated at 325 °C under an argon atmosphere, cooled down to room temperature, and transferred into a glovebox. The reaction tube was unsealed and the resulting solid mixture was characterized by PXRD.

Fabrication of devices for photocurrent measurements

In a glovebox, the perovskite powder sample (300 mg) was placed between two stainless steel pellets in a hydraulic press and compressed with a force of 10^4 kg for 15 m. One of the resultant sample discs is shown in Figure 7(a). A typical sample disc is 2 mm in thickness. Each disc was then sealed in a 20 mL vial, placed into an air-tight Ziploc bag, and then transferred to the laboratory for the gold electrodes to be deposited.

Powder X-ray diffraction study

Measurements were performed on a Rigaku SmartLab X-ray diffractometer, fitted with a copper ($K_{\alpha1}$ (1.54059)/$K_{\alpha2}$ (1.54441) = 2) target X-ray tube set to 40 kV and 30 mA and a SC-70 scintillation detector. A medium resolution parallel-beam (PB) cross beam optics (CBO) unit was used with a 10 mm slit width. The powder samples were packed in airtight specimen holders (Bruker A100B33) in a glovebox. The respective PXRD patterns were obtained for 2θ angles from 4° to 50° at 0.04° per step.

Ultraviolet-visible diffuse reflectance spectroscopic (UV-vis DRS) study

UV-vis spectra were acquired using a Shimadzu UV-3600 UV-vis spectrometer with an integrating sphere (Shimadzu ISR-3100). Powder samples were sealed in quartz cuvettes.

X-ray photoelectron spectroscopic (XPS) study

XPS data were acquired using a Phoibos 100 spectrometer and a Mg X-ray source (SPECS, Germany) working at 12.5 kV equipped with dual Al/Mg anodes. Samples were prepared by coating a uniform layer of the materials on SPI double-sided adhesive carbon tape in a glovebox. The samples were then removed from the glovebox sealed in a vial and transferred to the laboratory for the spectrometer. Although there was a brief

exposure of each sample (< 5 s) when it was loaded into the spectrometer, the sample was then evacuated to a pressure below 10^{-8} mbar. Remarkably, no noticeable oxidation was observed despite the fact that XPS is a surface-sensitive technique. The carbon tape contains acrylate adhesives, so both C 1s and O 1s signals are present in the carbon tape itself. The XPS data were processed using the CasaXPS software. The spectra were calibrated internally according to the adventitious C 1s position at 284.6 eV.

Photoluminescence spectroscopic study

Measurements were carried out and ultrafast femtosecond optical spectroscopic methods were employed to measure the PL data and FWHM of the thin films. A Coherent Libra regenerative amplifier (50 fs, 1 kHz, 800 nm) seeded by a Coherent Vitesse Oscillator (100 fs, 80 MHz) were used as the pump laser sources. For pump wavelength tuning, the Coherent OPerA Solo optical parametric amplifier was used. Upon optically pumping the samples, the respective PL emissions were collected at a backscattering angle of 150° by a collimating lens pair and guided into an optical fiber that was coupled to a spectrometer (Acton, SpectraPro 2500i and SP2300) and detected by a charge coupled device (CCD; Princeton Instruments, Pixis 400B). Time-resolved PL (TRPL) was collected using an Optronis Optoscope streak camera system. For the spin-coated samples, 1:1 stoichiometric amounts of the respective salts were dissolved in DMF and spin-coated on 1x1 cm plasma-treated quartz substrates. The samples were then annealed at 373 K under a N_2 atmosphere. Due to the moisture sensitivity of the perovskites prepared, all samples were sealed into air-tight quartz cuvettes inside a glovebox. The optical measurements were performed at room temperature (295-298 K) under ambient pressures.

Photoelectrical study

Photoelectrical measurements were carried out using a Keithley 4200-SCS semiconductor characterization system with a coupled light source (Thorlabs Solis-445C) and a DC2200 driver. For each as-prepared perovskite pellet, the sample was removed from the vial, loaded, and then evacuated so that 200 nm thick gold electrodes could be deposited through thermal evaporation using shadow masks (active device area: 4000 µm × 200 µm = 8×10^{-7} m^2). The light source was operating at an intensity of 693.1 W/m^2. Detectivity is calculated using the formula below:

$$\textbf{Detectivity} = \textbf{Responsivity} \times \sqrt{\frac{\textbf{Device area}}{2e \times I_{dark}}}$$

Supplemental References

Askar, A.M., Karmakar, A., Bernard, G.M., Ha, M., Terskikh, V.V., Wiltshire, B.D., Patel, S., Fleet, J., Shankar, K., and Michaelis, V.K. (2018). Composition-Tunable Formamidinium Lead Mixed Halide Perovskites via Solvent-Free Mechanochemical Synthesis: Decoding the Pb Environments Using Solid-State NMR Spectroscopy. J Phys Chem Lett *9*, 2671-2677.

El Ajjouri, Y., Chirvony, V.S., Sessolo, M., Palazon, F., and Bolink, H.J. (2018a). Incorporation of potassium halides in the mechanosynthesis of inorganic perovskites: feasibility and limitations of ion-replacement and trap passivation. RSC Adv *8*, 41548-41551.

El Ajjouri, Y., Palazon, F., Sessolo, M., and Bolink, H.J. (2018b). Single-Source Vacuum Deposition of Mechanosynthesized Inorganic Halide Perovskites. Chem Mater *30*, 7423-7427.

Jana, A., Mittal, M., Singla, A., and Sapra, S. (2017). Solvent-free, mechanochemical syntheses of bulk trihalide perovskites and their nanoparticles. Chem Commun *53*, 3046-3049.

Karmakar, A., Askar, A.M., Bernard, G.M., Terskikh, V.V., Ha, M., Patel, S., Shankar, K., and Michaelis, V.K. (2018). Mechanochemical Synthesis of Methylammonium Lead Mixed–Halide Perovskites: Unraveling the Solid-Solution Behavior Using Solid-State NMR. Chem Mater *30*, 2309-2321.

Pal, P., Saha, S., Banik, A., Sarkar, A., and Biswas, K. (2018). All-Solid-State Mechanochemical Synthesis and Post-Synthetic Transformation of Inorganic Perovskite-type Halides. Chem Eur J *24*, 1811-1815.

Posudievsky, O.Y., Konoshchuk, N.V., Karbivskyy, V.L., Boiko, O.P., Koshechko, V.G., and Pokhodenko, V.D. (2017). Structural and Spectral Characteristics of Mechanochemically Prepared CsPbBr3. Theor Exp Chem *53*, 235-243.

Prochowicz, D., Yadav, P., Saliba, M., Kubicki, D.J., Tavakoli, M.M., Zakeeruddin, S.M., Lewiński, J., Emsley, L., and Grätzel, M. (2018). One-step mechanochemical incorporation of an insoluble cesium additive for high performance planar heterojunction solar cells. Nano Energy *49*, 523-528.

Prochowicz, D., Yadav, P., Saliba, M., Saski, M., Zakeeruddin, S.M., Lewiński, J., and Grätzel, M. (2017). Mechanosynthesis of pure phase mixed-cation MAxFA1−xPbI3 hybrid perovskites: photovoltaic performance and electrochemical properties. Sustainable Energy Fuels *1*, 689-693.

Protesescu, L., Yakunin, S., Nazarenko, O., Dirin, D.N., and Kovalenko, M.V. (2018). Low-Cost Synthesis of Highly Luminescent Colloidal Lead Halide Perovskite Nanocrystals by Wet Ball Milling. ACS Appl Nano Mater *1*, 1300-1308.

Sadhukhan, P., Kundu, S., Roy, A., Ray, A., Maji, P., Dutta, H., Pradhan, S.K., and Das, S. (2018). Solvent-Free Solid-State Synthesis of High Yield Mixed Halide Perovskites for Easily Tunable Composition and Band Gap. Cryst Growth Des *18*, 3428-3432.

Yun, S., Kirakosyan, A., Yoon, S.-G., and Choi, J. (2018). Scalable Synthesis of Exfoliated Organometal Halide Perovskite Nanocrystals by Ligand-Assisted Ball Milling. ACS Sustainable Chem Eng *6*, 3733-3738.